AGU PUBLICATIONS

JGR

Journal of Geophysical Research: Oceans

RESEARCH ARTICLE

10.1002/2016JC012403

Special Section:
Atmosphere-ice-ocean-ecosystem Processes in a Thinner Arctic Sea Ice Regime: the Norwegian Young Sea ICE Cruise 2015 (N-ICE2015)

Thin ice and storms: Sea ice deformation from buoy arrays deployed during N-ICE2015

Polona Itkin[1], Gunnar Spreen[1,2], Bin Cheng[3], Martin Doble[4], Fanny Girard-Ardhuin[5], Jari Haapala[3], Nick Hughes[6], Lars Kaleschke[7], Marcel Nicolaus[8], and Jeremy Wilkinson[9]

[1]Norwegian Polar Institute, Tromsø, Norway, [2]Institute of Environmental Physics, University of Bremen, Bremen, Germany, [3]Finnish Meteorological Institute, Helsinki, Finland, [4]Polar Scientific Ltd., Argyll, UK, [5]Laboratoire d'Océanographie Physique et Spatiale, IFREMER, Plouzane, France, [6]Norwegian Meteorological Institute, Tromsø, Norway, [7]Institute of Oceanography, University of Hamburg, Hamburg, Germany, [8]Alfred-Wegener-Institut Helmholtz-Zentrum für Polar- und Meeresforschung, Bremerhaven, Germany, [9]British Antarctic Survey, Cambridge, UK

Abstract Arctic sea ice has displayed significant thinning as well as an increase in drift speed in recent years. Taken together this suggests an associated rise in sea ice deformation rate. A winter and spring expedition to the sea ice covered region north of Svalbard–the Norwegian young sea ICE2015 expedition (N-ICE2015)—gave an opportunity to deploy extensive buoy arrays and to monitor the deformation of the first-year and second-year ice now common in the majority of the Arctic Basin. During the 5 month long expedition, the ice cover underwent several strong deformation events, including a powerful storm in early February that damaged the ice cover irreversibly. The values of total deformation measured during N-ICE2015 exceed previously measured values in the Arctic Basin at similar scales: At 100 km scale, N-ICE2015 values averaged above 0.1 d^{-1}, compared to rates of 0.08 d^{-1} or less for previous buoy arrays. The exponent of the power law between the deformation length scale and total deformation developed over the season from 0.37 to 0.54 with an abrupt increase immediately after the early February storm, indicating a weakened ice cover with more free drift of the sea ice floes. Our results point to a general increase in deformation associated with the younger and thinner Arctic sea ice and to a potentially destructive role of winter storms.

Key Points:
- Two buoy arrays deployed in winter and spring 2015 showed very high sea ice deformation rates north of Svalbard
- A storm event in early February irreversibly damaged the sea ice cover adjacent to the marginal ice zone
- Single winter storm events, penetrating deep in the sea ice, can permanently precondition the sea ice cover for the subsequent melting

Correspondence to:
P. Itkin,
Polona.Itkin@npolar.no

Citation:
Itkin, P., G. Spreen, B. Cheng, M. Doble, F. Girard-Ardhuin, J. Haapala, N. Hughes, L. Kaleschke, M. Nicolaus, and J. Wilkinson (2017), Thin ice and storms: Sea ice deformation from buoy arrays deployed during N-ICE2015, *J. Geophys. Res. Oceans*, *122*, 4661–4674, doi:10.1002/2016JC012403.

Received 3 OCT 2016
Accepted 13 MAR 2017
Accepted article online 17 MAR 2017
Published online 8 JUN 2017

1. Introduction

In addition to a remarkable shrinking and thinning [*Arctic Monitoring and Assessment Programme*, 2013], the drift speed of the Arctic pack ice has increased, even though the wind forcing has remained of similar magnitude [*Rampal et al.*, 2009; *Spreen et al.*, 2011]. This has been ascribed to the reduced material strength of the thinner ice. The wind and ocean driven sea ice drift are not uniform and the differential motion causes the ice to break and deform in features such as pressure ridges and leads. When the sea ice starts to melt in summer these features are the weak points along which the ice cover disintegrates [*Perovich et al.*, 2001; *Arntsen et al.*, 2015]. The summer sea ice extent can be additionally impacted by the storms and swell [*Asplin et al.*, 2012; *Zhang et al.*, 2013], but much of it is preconditioned by the sea ice dynamics during the cold season [e.g., *Kauker et al.*, 2009; *Kimura et al.*, 2013]. With higher drift speeds and weaker sea ice, we expect more sea ice deformation that will have positive feedback on the sea ice mass balance, at least during winter, freezing conditions. During the melting season the more fractured sea ice that provides more surface for lateral melt and allows stronger wave penetration, can have an opposite effect, i.e., increased ice melting and thereby decrease in the ice volume.

Sea ice deformation depends strongly on local ice conditions and the weather. This makes a straightforward analysis difficult and statistical approaches must be used. Previous studies of deformation using a combination of satellite remote sensing data and buoy deployments [e.g., *Marsan et al.*, 2004; *Stern and Lindsay*, 2009; *Hutchings et al.*, 2011] described a power law relationship between deformation and the spatial scale on which it is measured. The law $D=aL^{-\beta}$, where D and L are deformation and length scale, while a and β are constants indicates that deformation is spatially concentrated in small areas surrounded by vast undeformed regions. Deformation processes occur predominantly along long, narrow areas spanning up to few hundred kilometers, commonly termed linear kinematic features. If a small area contains an active deformation feature, the deformation value calculated for that area will be higher than for a larger area that contains

the same feature, since the larger area contains a significant portion of undeformed sea ice. Knowing the β exponent of the power law we can statistically estimate the low spatial resolution values based on measurements of the high resolution total deformation and vice versa. This is essential for comparing, e.g., small scale in situ measurements to larger scale satellite based products, or to numerical model deformation estimates. Another use of β is that its value varies according to the degree of localization of deformation. An increase of β value in time means that deformation is reduced at shorter spatial scales, which indicates reduced sea ice strength typical for warmer ice and free drift conditions. The value of β typically increases during the winter-summer transition [*Stern and Lindsay*, 2009] and depends on temperature [*Oikkonen et al*., 2016] and distance from the ice edge [*Oikkonen et al*., 2017].

The winter sea ice remains logistically hard to access and winter in situ data are scarce. The sea ice covered region north of Svalbard is part of the Transpolar Drift system and is characterized by relatively high sea ice drift speeds, proximity to the ice edge, and lately also by the large fraction of first year sea ice, typically originating from the vast areas of Siberian shelf seas [*Renner et al*., 2014]. The relative accessibility of this area during the winter makes it an ideal study region for sea ice dynamics in the new Arctic. The region was studied during the Norwegian young sea ICE (N-ICE2015) expedition [*Granskog et al*., 2016] in the first half of 2015. N-ICE2015 was a multidisciplinary expedition that collected data from the Arctic atmosphere, ocean, sea ice, and ecosystem [*Cohen et al*., 2017; *Meyer et al*., 2017; *Provost et al*., 2017; *Olsen et al*., 2017]. The research work was based around the Norwegian Polar Institute research vessel *Lance* that was assisted to around 83°N by the Norwegian coastguard ice-breaker *KV Svalbard* on four occasions and left to drift passively southward toward the ice edge.

The current study concentrates on buoy data from two of such southward drifts. A total of 42 buoys (Tables 1 and 2) were deployed in nested arrays at spacings of 5–100 km, separated into a winter deployment in January/February and a spring deployment in April/May. Instruments were placed on a mixture of first-year and second-year ice that was characteristic for the region. The sea ice in the array was relatively thin with modal thicknesses between 0.9 and 1.7 m and covered by snow with mean depth between 0.3 and 0.5 m [*Rösel et al*., 2016a,2016b]. Sea ice deformation on a smaller scale was simultaneously studied by analyzing ship radar images [*Oikkonen et al*., 2017]. We compare our results to several previous studies which deployed buoy arrays (Figure 1) in late winter and spring in the 2000s: ACSYS in 2003 (Transpolar Drift north of Svalbard, 10 buoys deployed in April 2003), DAMOCLES in 2007 (North Pole region, 16 buoys deployed in April 2007), and SEDNA in 2007 (Beaufort Sea, 12 buoys deployed in March 2007). While the deployment times of these arrays overlap, the

Table 1. List of the Buoys Deployed as Part of the Winter Buoy Array During the N-ICE2015 Expedition[a]

Name	Type	Deployment Date	Deployment Location	Total Duration (Days)	Distance Covered (km)	Average Speed (m/s)	IMEI
CALIB_2015a[b]	Drifter	28 Jan 2015	N83.0902 E17.7636	45	721	0.5490	300234062447630
CALIB_2015b[b]	Drifter	21 Jan 2015	N83.1588 E20.0232	53	889	0.5770	300234062440630
CALIB_2015d[b]	Drifter	17 Jan 2015	N83.2120 E20.7078	56	888	0.5427	300234061362150
CALIB_2015e[b]	Drifter	10 Feb 2015	N82.3630 E18.9038	32	534	0.5666	300234061369130
CALIB_2015f[b]	Drifter	20 Jan 2015	N83.1762 E20.0984	0	2	0.1364	300234061269230
SNOW_2015a	Snow buoy	25 Jan 2015	N83.0138 E19.8446	27	442	0.1895	300234062311650
SVP_2015a	Drifter	18 Jan 2015	N83.2238 E21.0196	95	2109	0.2579	300234062447650
SVP_2015c[b]	Drifter	30 Jan 2015	N83.0382 E16.7684	44	758	0.5953	300234011090780
SIMBA_2015a	IMB	14 Jan 2015	N83.2463 E21.6447	60	1014	0.1935	300234061263830
SIMBA_2015b[c]	IMB	15 Jan 2015	N83.0458 E21.9495	42	660	0.1815	300234062420090
SIMBA_2015e[c]	IMB	26 Jan 2015	N83.0472 E18.7160	3 (25)[d]	Unknown	Unknown	300234060695050
SIMBA_2015f[c]	IMB	25 Jan 2015	N83.0138 E19.8446	27	442	0.1895	300234011383170
SIMBA_2015g	IMB	29 Jan 2015	N83.0905 E17.0404	42	846	0.2322	300234060666760
WAVE_2015a[c]	Wave buoy	15 Jan 2015	N83.1691 E21.3318	21	85	0.2116	300025010247350
WAVE_2015b	Wave buoy	16 Jan 2015	N82.6767 E23.2338	39	620	0.1940	300025010343830
WAVE_2015c	Wave buoy	16 Jan 2015	N82.3456 E24.8132	30	513	0.2081	300025010249350
WAVE_2015d	Wave buoy	16 Jan 2015	N82.0115 E25.4361	15	182	0.1485	300025010340820
STRESS_2015a[c]	Stress buoy	25 Jan 2015	N83.0138 E19.8446	27	442	0.1895	300034013532140
IMB_2015a	IMB	18 Jan 2015	N82.9843 E21.5213	42	660	0.1815	300025000000000

[a]Duration of the buoy deployment is estimated until end of data transmission or to the point when the drift speed exceeded 2 m/s. Distance is calculated based on the recorded displacements and does not account for the motion in between.
[b]Buoys with 3 hourly GPS position.
[c]Buoys not used for the sea ice deformation calculation.
[d]GPS antenna failed soon after deployment. Iridium position and data available for number of days in brackets.

Table 2. List of the Buoys Deployed as Part of the Spring Buoy Array During the N-ICE2015 Expedition[a]

Name	Type	Deployment Date	Deployment Location	Total Duration (Days)	Distance Covered (km)	Average Speed (m/s)	IMEI
CALIB_2015c[b]	Drifter	21 Apr 2015	N82.9660 E16.4936	43	486	0.3891	300234061371430
CALIB_2015g[b]	Drifter	21 Apr 2015	N82.9242 E16.1952	46	594	0.4463	300234061369140
SNOW_2015d	Snow buoy	1 Mar 2015	N82.9480 E26.4312	66	904	0.1582	300234062424060
SNOW_2015b	Snow buoy	23 Apr 2015	N82.7944 E16.2662	46	613	0.1518	300234062311650
SNOW_2015c	Snow buoy	20 Apr 2015	N83.1798 E16.3920	51	659	0.1470	300234062426060
SNOW_2015e	Snow buoy	21 Apr 2015	N83.0042 E16.0852	49	654	0.1521	300234062426150
SVP_2015b	Drifter	20 Apr 2015	N82.8952 E14.0812	44	569	0.1497	300234062442640
SVP_2015d[b]	Drifter	27 Apr 2015	N82.4800 E14.1466	44	566	0.4394	300234010080470
SVP_2015e[b]	Drifter	20 Apr 2015	N83.0500 E15.0496	51	695	0.4702	300234010084440
SVP_2015f[b]	Drifter	20 Apr 2015	N83.0506 E15.0672	50	633	0.4342	300234011091510
AFAR_2015a	Radiation buoy	4 May 2015	N82.0044 E11.5790	39	548	0.1589	300234062726310
AFAR_2015b	Radiation buoy	4 May 2015	N82.0920 E13.0624	38	542	0.1620	300234062317630
AFAR_2015c	Radiation buoy	8 May 2015	N81.5956 E10.1742	32	374	0.1333	300234062722280
SIMBA_2015c	IMB	22 Apr 2015	N82.8610 E16.5697	48	669	0.1587	300234061760870
SIMBA_2015d	IMB	7 Mar 2015	N83.1578 E23.7701	77	1562	0.2342	300234061762880
WAVE_2015e	Wave buoy	17 Apr 2015	N83.0534 E13.3942	36	450	0.1512	300025010345830
WAVE_2015f	Wave buoy	17 Apr 2015	N82.4555 E17.7205	39	620	0.1930	300025010241360
IMB-B_2015a[c]	IMB	4 May 2015	N82.0885 E13.0590	25	264	0.1277	300025010735970
IMB-B_2015b[c]	IMB	8 May 2015	N81.5660 E9.9498	22	240	0.1293	300025010738970
IMB-B_2015c[c]	IMB	4 May 2015	N82.0044 E11.5786	30	315	0.1541	300025010731970
RIDGE_2015a[c]	Ridge IMB	29 Apr 2015	N82.0488 E13.4294	22	210	0.1129	300234061879260
RIDGE_2015b[c]	Ridge IMB	12 Jun 2015	N80.7645 E12.0827	17	310	0.2116	300234061874260
IMB-S_2015a[c,d]	Seasonal IMB	19 May 2015	N82.2333 E10.3226	117	Unknown	Unknown	300234061666330
IC_2015a[c]	Drifter	21 Apr 2015	N82.9 E16.7	52	Unknown	Unknown	Argos

[a]Duration of the buoy deployment is estimated until end of data transmission or to the point when the drift speed exceeded 2 m/s. Distance is calculated based on the recorded displacements and does not account for the motion in between.
[b]Buoys with 3 hourly GPS position.
[c]Buoys not used for the sea ice deformation calculation.
[d]Buoys with 6 hourly GPS position.

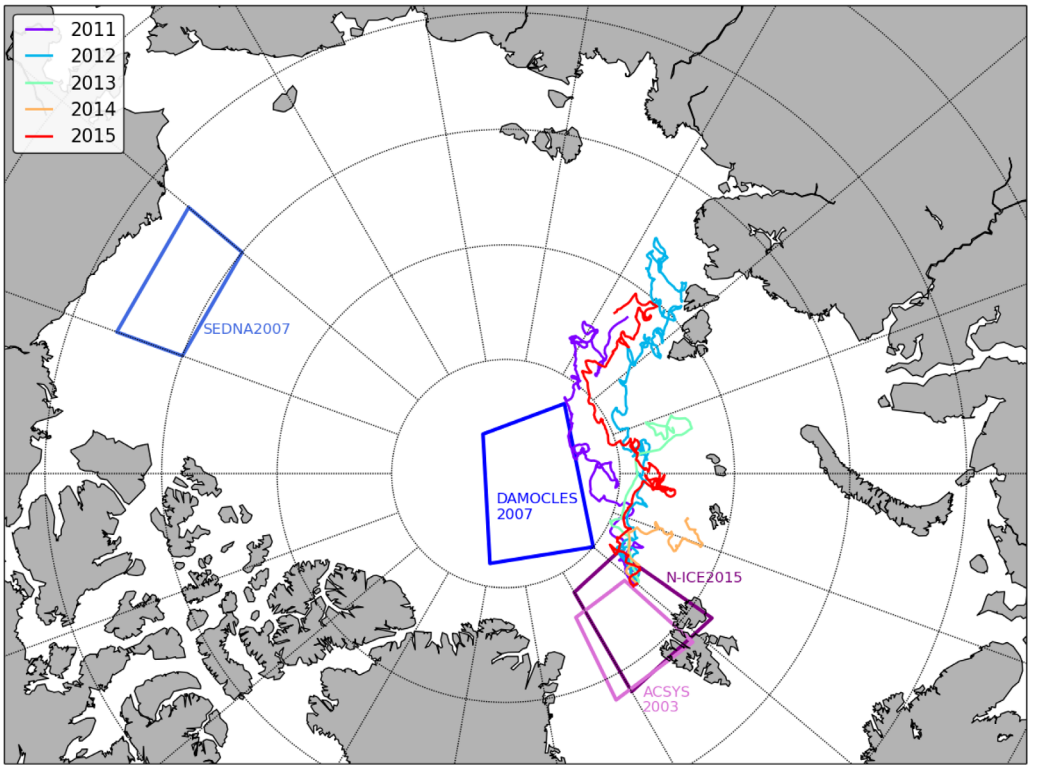

Figure 1. Back trajectories of the sea ice in the N-ICE2015 region for recent years (2011–2015) show the typical origin of the ice in that region. Regions of buoy arrays used in this study (N-ICE2015, SEDNA2007, ACSYS2003, and DAMOCLES2007) are shown as boxes.

N-ICE2015 winter array starts considerably earlier in the season than these previous efforts, which allows new insights.

In this paper, we present the sea ice buoy data collected during N-ICE2015, study the sea ice dynamics based on these data explore the temporal development of the sea ice deformation processes, connect the information to the previous studies and propose links between the differences observed and changes in the Arctic sea ice cover and climate.

2. Methods and Data

2.1. Buoy Data

Winter and spring deployments both aimed to create multiscale buoy arrays for the dynamics study described here and for other scientific aims. As such, a wide range of instrument types were used, though these were dominantly on-ice beacons that sank once their supporting ice floe disintegrated. In this paper, we refer to these instruments as "buoys." All are listed in Tables 1 and 2. The buoy types included simple drifters—Compact Air-Launched Ice Beacon (CALIB), surface velocity profilers (SVP) and ice beacon drifters (IC) all produced by MetOcean, Halifax Canada, snow beacons (SNOW, produced by MetOcean), four types of sea Ice Mass balance Buoys (IMBs) including SIMBA units (SAMS Research Services Ltd. (SRSL), Oban, Scotland, IMB-Bs (Bruncin, Zagreb, Croatia), an IMB (MetOcean) and a seasonal IMB-S (Cold Regions Research and Engineering Laboratory (CRREL), Hanover, USA), radiation buoys (Affordable Arctic Radiation drifter—AFAR, MetOcean), wave buoys (Bruncin), ridge IMB buoys (RIDGE, Oceanic Thermistor Buoy Model 908 produced by Oceanic Measurement, Sydney, Canada), and a sea ice stress buoy (STRESS, CRREL). Logistics for the two deployment groups were very different: The winter array was deployed during polar night with the assistance of KV Svalbard, snow machines and hauling by ski, which limited the possibilities of constructing a large and symmetric array. The spring array was deployed from a helicopter and *Lance*, resulting in it being more symmetric with clearly distinguishable inner and outer rings. For both deployments, the buoys were deployed over approximately 1 month and had a relatively short lifetime of up to 3 months. Some buoys stopped functioning before the array was finished. For the drifters with flotation support such as the SVPs, we take the first occurrence of a drift speed greater than 2 m/s as the point when the buoy was no longer drifting on ice. Buoys with the longest deployment duration also had the highest drift speeds, since velocities increased toward the ice edge.

The winter array drifted in south and south-east directions with some buoys traveling over 1000 km (Figure 2). The spring array drifted southwestward, with a track length of almost 700 km. The distance is calculated based on the hourly positions of the buoys and does not take into account additional meandering between the measurements. Many buoys were deployed in co-located clusters and neighboring buoys' GPS locations were used in the event of a nearby buoy's GPS failure, which happened for several IMBs. One buoy was selected from each cluster or pair of buoys for the deformation calculations. Positions from a total of 13 and 16 buoys were used to construct the sea ice deformation array for the winter and spring deployment, respectively. All buoy positions and IMB data acquired during N-ICE2015 are publicly available at http://data.npolar.no [*Itkin et al*., 2015] and partly also at http://www.meereisportal.de. The IMB data from N-ICE2015 are described and analyzed in a separate paper by *Provost et al*. [2017].

2.2. Sea Ice Conditions and Origin

To understand the age and origin of ice in the study region and compare ice conditions with previous years, we tracked the ice back in time with a coarse resolution ice drift from satellite observations. We used daily ice motion vectors based on ASCAT scatterometer and SSM/I radiometer data [*Girard-Ardhuin and Ezraty*, 2012] for the winter months and bridged the gap in ice drift data during the summer months by using an unpublished version of summer ASCAT/SSMIS ice drift data by the same provider. Ice was tracked back to its origin for the 5 years between 2011 and 2015 always starting on 15 March of each year at 82.5°N and 20°E (Figure 1). The ice drift at a given position is obtained from the 62.5 km large grid cell of the ASCAT/SSMI drift data set covering that position. The previous day's position is estimated from that drift vector and the procedure is repeated going back in time until either land or ice concentrations below 15% for more than 1 day are encountered. Due to the low resolution of the ice drift data and some gaps in the ice drift fields, especially during summer, the ice back-trajectory will diverge from the real trajectory and have some uncertainty. This approach is suitable to determine the sea-ice source region within an approximately

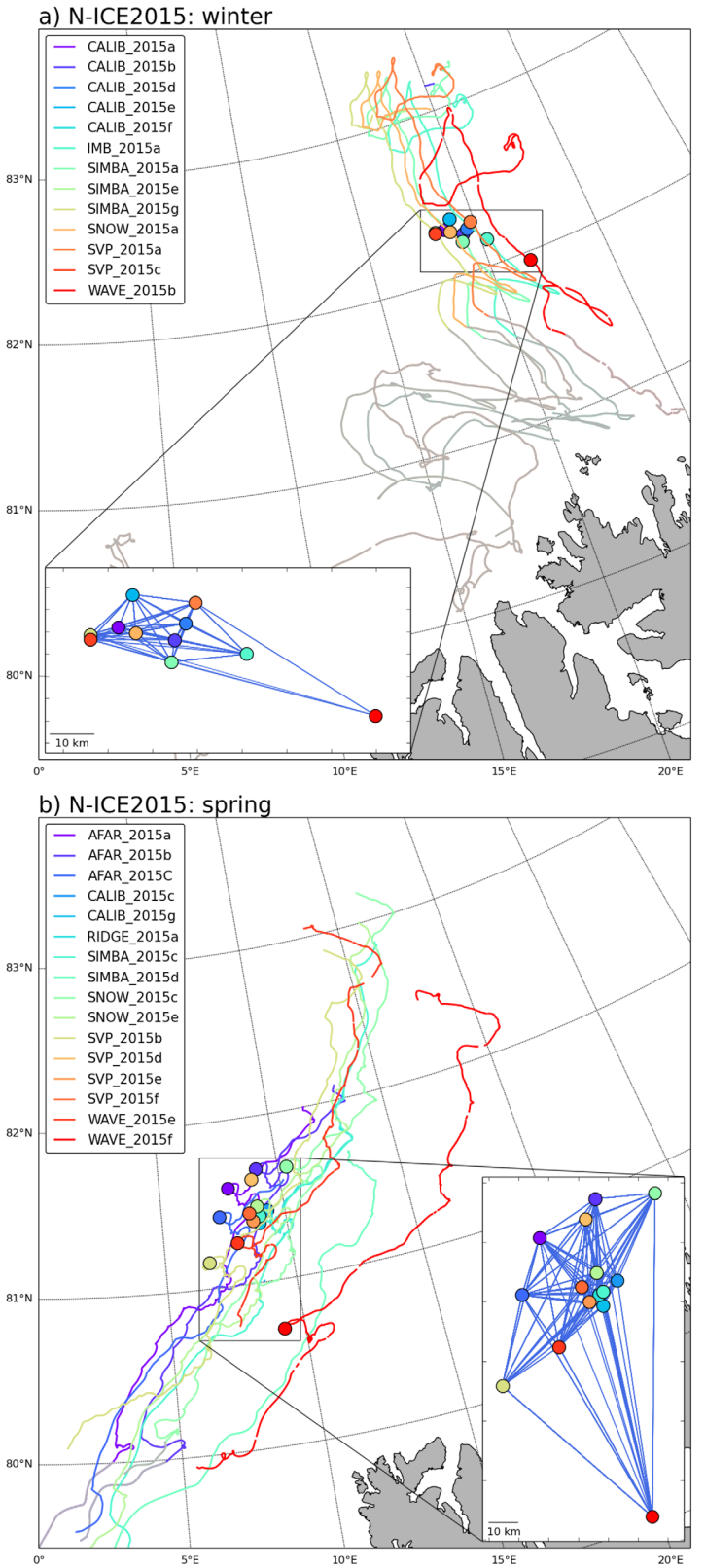

Figure 2. Buoy drift tracks for the (top) winter and (bottom) spring deployment. Only buoys used for the deformation calculations are shown. The position of the buoys on 2 February 2015 and 15 May 2015 is depicted by circles. By those dates all the buoys were deployed, but some had already ceased transmission. The triangles used for the deformation calculation are outlined by blue lines in the magnified map of the array. The buoy tracks after the breakup are shaded in gray.

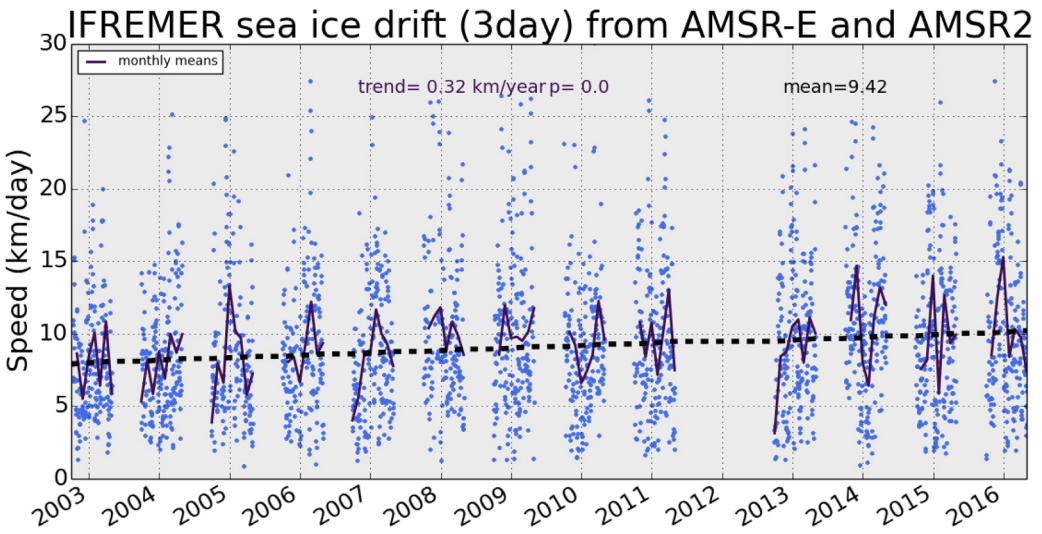

Figure 3. Time series of sea ice drift speeds, with monthly means and overall trend, in the N-ICE2015 region during winter (October to April) for the period 2003–2016.

100 km radius. The back-tracking algorithm does not consider new ice growth, i.e. the presented trajectories represent the oldest ice for that region. It does not contain any information of the ice age composition and younger ice can also be present. The backtracking results show that between 2011 and 2015 sea ice in the region was typically a mixture of second year ice—mainly formed in the Laptev Sea—and first year ice (2011, 2012, and 2015) or exclusively first year ice formed in the northern Barents Sea (2013 and 2014). The in situ observations confirmed presence of the older sea ice within the N-ICE2015 buoy arrays [*Granskog et al*., 2017], though the ice pack was predominantly first year ice.

Older sea ice is typically thicker and stronger than first year ice. To explore the influence of the ice age on the sea ice dynamics we looked at the sea ice drift speed trends in the area north of Svalbard since 2002. We analyzed a higher spatial resolution sea ice drift (31.25 km) based on AMSR-E and AMSR2 passive microwave data available during winter months [*Girard-Ardhuin and Ezraty*, 2012]. The results of this product with 3 day resolution (Figure 3) show that although the sea ice drift speed in the N-ICE2015 region follows an increasing trend since 2003, the speeds in 2015 were lower than during years with exclusively first year ice (2013 and 2014). This implies that our study provides a lower bound for the deformation rates during recent years in the area.

As an auxiliary data set to interpret the sea ice drift and deformation time series from the N-ICE2015 arrays, we estimated the distance to the ice edge from the navigational sea ice charts produced by the Norwegian Meteorological Institute. The charts were updated with near-daily frequency by visual analysis of Synthetic Aperture Radar (SAR) images. We calculated the shortest distance between the center of the array (*Lance*) and the inner edge of the ice class "open water." The distance between the buoy array and the ice edge started just below 200 km and it gradually decreased to zero for both arrays.

2.3. Deformation Calculation

Deformation rates were calculated from triangles (Figure 2) formed between the buoys (numbered 1–3 in the equations below). Following *Hutchings et al*. [2012], the Green's Theorem was used to calculate strain rates within the triangles defined by line integrals. For every buoy, we projected its position at every time step to a geographical grid to obtain zonal and meridional coordinates (x,y). Velocities of a buoy (u,v) at a given time step were estimated based on the displacements from the position of the previous time step. Since triangles with very acute angles give inaccurate results, only triangles with all the internal angles greater than 15° were used for the analysis. In contrast to the method used by *Hutchings et al*. [2011], we did not predefine or follow individual shapes, but we estimated the strain rate components $\frac{\partial u}{\partial x}$, $\frac{\partial u}{\partial y}$, $\frac{\partial v}{\partial x}$ and $\frac{\partial v}{\partial y}$ for all possible triangles that satisfy the minimum angle criterion and with vertices arranged in a counterclockwise order at every time step as:

$$\frac{\partial u}{\partial x}=\frac{1}{2A}[(u_1+u_3)(y_1-y_3)+(u_1+u_2)(y_1-y_2)+(u_2+u_3)(y_2-y_3)], \quad (1)$$

$$\frac{\partial u}{\partial y}=-\frac{1}{2A}[(u_1+u_3)(x_1-x_3)+(u_1+u_2)(x_1-x_2)+(u_2+u_3)(x_2-x_3)], \quad (2)$$

$$\frac{\partial v}{\partial x}=\frac{1}{2A}[(v_1+v_3)(y_1-y_3)+(v_1+v_2)(y_1-y_2)+(v_2+v_3)(y_2-y_3)], \quad (3)$$

$$\frac{\partial v}{\partial y}=-\frac{1}{2A}[(v_1+v_3)(x_1-x_3)+(v_1+v_2)(x_1-x_2)+(v_2+v_3)(x_2-x_3)], \quad (4)$$

where A is the triangle area. The divergence div is defined as:

$$div=\frac{\partial u}{\partial x}+\frac{\partial v}{\partial y} \quad (5)$$

and maximal shear rate shr as:

$$shr=\sqrt{\left(\frac{\partial u}{\partial x}-\frac{\partial v}{\partial y}\right)^2+\left(\frac{\partial u}{dy}+\frac{\partial v}{\partial x}\right)^2}. \quad (6)$$

The GPS receivers were programmed to sample on the hour, though some clock drift was evident for several buoys. We linearly interpolated (assuming constant drift speed and direction) the position of any such instruments to the hour before using it in the calculations. Also, while the majority of the N-ICE2015 buoys were providing GPS positions every hour, some were only sampling every 3 h (Tables 1 and 2). To be able to use all the data, we constructed the time series of deformation from the buoys with hourly data and then downscaled all the data to 3 hourly resolution to obtain as many data points as possible for estimates of total deformation, defined as $D=\sqrt{div^2+shr^2}$. The total deformation was used to assess the scaling law in sea ice deformation where

$$D \propto L^{-\beta} \quad (7)$$

and $L=\sqrt{A}$. For this task, we did not bin the triangles in length scale L classes. Instead we fitted the function to all individual data points. This enables a more robust fit with narrower confidence bands.

The buoy manufacturers have estimated the positioning error δ_x of stationary buoy to be around 25 m. For a moving platform δ_x increases thus we take δ_x as 50 m to be a conservative estimate. The velocity error can be estimated as $\delta_U=\frac{\sqrt{2}\delta_x}{T}$ [*Hutchings et al.*, 2012], which gives a value of 0.01 m/s. All the cases when a certain buoy was moving with a velocity lower than this were excluded from the analysis. According to *Hutchings et al.* [2012], the error of the deformation estimate becomes negligible when $A \gg 8N^2\delta_x^2$, where N is the number of buoys in the polygon. Our smallest L is about 2 km, which means that if $\delta_x < 235$ m our deformation estimates has reasonable signal-to-noise ratio.

3. Sea Ice Deformation in Connection to the Storms and Breakup Events During N-ICE2015

The time series in Figure 4 shows sea ice drift and deformation along with the most important forcing (wind and air temperatures) distance to the sea ice edge and sea ice concentration. The temperature and wind data shown on the figure are observations from the meteorological mast at 2 and 10 m [*Cohen et al.*, 2017] positioned approximately in the center of the array. Storms are indicated in blue and purple shading. These are defined *Cohen et al.* [2017] as events with wind speeds greater than 8 m/s for a duration of at least three hours with breaks not longer than one hour. Storms are divided the storms to minor and major, where only latter have a pressure decrease of more than 5 hPa in six hours. Divergence and shear in the time series are shown for two extreme scales of the array: the averages of the triangles with length scale (1) smaller than 15 km and; (2) greater than 60 km. Deformation at both scales is coherent and the peaks at the small scale are typically higher than at the large scale, which is the consequence of the deformation localization. Moving averages with a 24 h window were used to smooth the deformation time series and distinguish between predominantly divergent and convergent regimes.

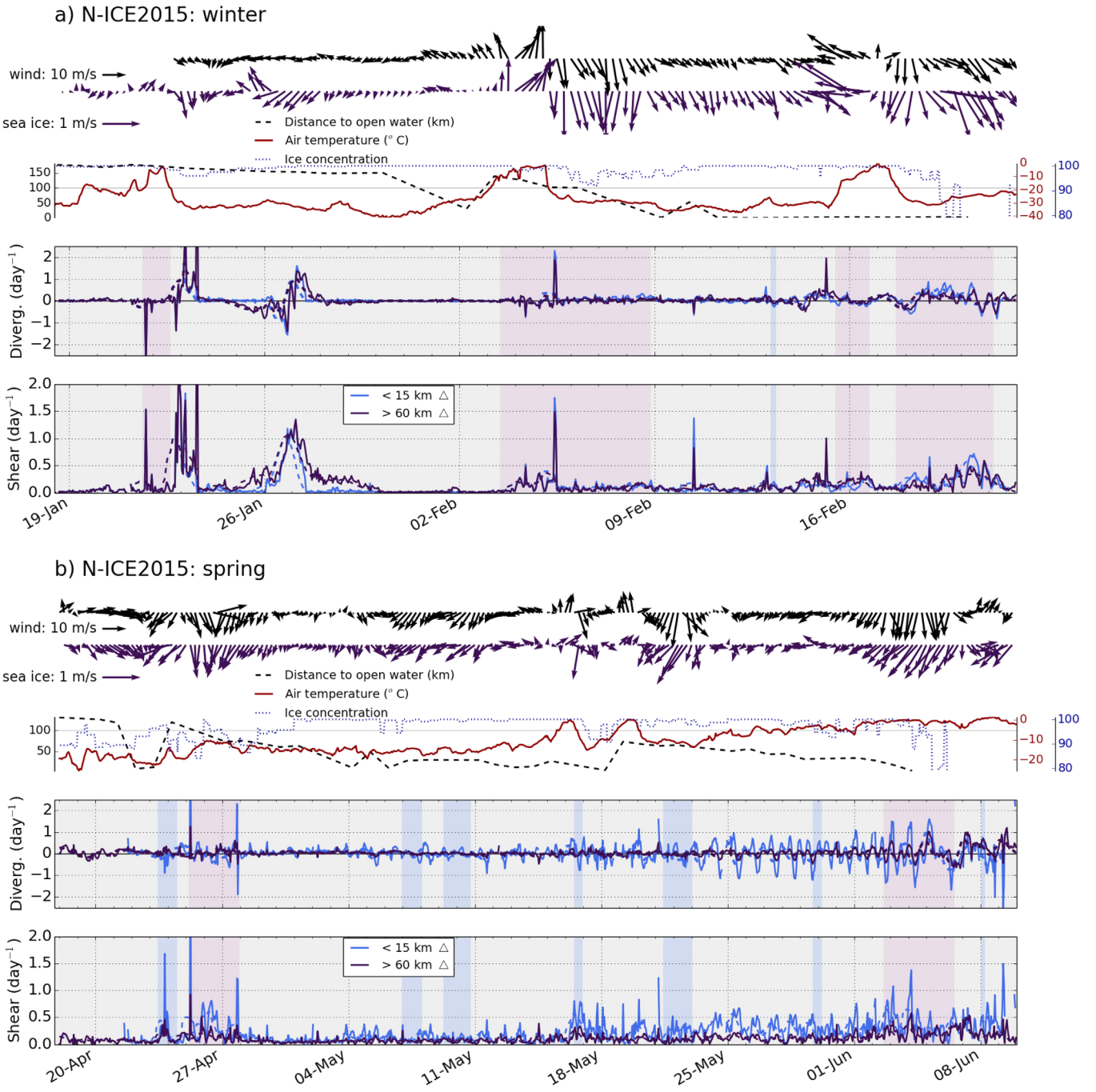

Figure 4. Mean sea ice drift, wind speed, distance from the open water, sea ice concentration, air temperature, divergence, and shear during the (top) winter and (bottom) spring deployment. Areas shaded in purple and blue are major and minor storms. Sea ice drift is the average of all the buoys in the array and the wind data are from the meteorological mast in the center of the array. On the divergence and shear plots solid blue line is the average calculated for the small scale triangles (length scale smaller than 15 km) and solid purple lines are the averages for the big triangles (length scale greater than 60 km). Dashed lines are the running means with 24 h averaging window.

The sea ice deformation measured by the N-ICE2015 buoys during the early part of the winter deployment peaked during storms and wind direction changes (e.g., event on 27th January that could be a consequence of a distant storm passing), but was close to zero between events. This may indicate rapid healing of the sea ice cover, as previously described for the Arctic winter [*Hutchings et al.*, 2011]. Sea ice drift had a mean speed of 0.33 m/s, which is high compared to the January to May climatological drift speed of about 0.02 m/s in the whole Arctic Ocean (https://nsidc.org/data/docs/daac/nsidc0116_

icemotion.gd.html) and had variable direction. As the buoys were in the Transpolar Drift current, and relatively close to the ice edge, the drift speed is expected to be higher than the Arctic as a whole, but the size of the difference was surprising. An unusually powerful storm between 3 and 8 February set the sea ice in even faster motion and opened large leads in the center of the buoy array [*Oikkonen et al*., 2017]. The storm resulted from an unusual extension of the polar vortex toward southern Greenland. This displaced the jet stream associated with winds blowing along the Greenland coast northward, carrying cyclones with warm air and moisture into the high Arctic [*Cohen et al*., 2017]. Strong southerly winds followed by strong northerly winds compressed and then opened up the sea ice north of Svalbard. During this time, the ice experienced a peak in convergence and shear followed by a strong peak in divergence (approximately 2 d^{-1}) and shear. The first peak indicated that the sea ice pressure was released by formation of pressure ridges in the shear zones. During the second peak the ice pack opened again and leads were formed. This is also reflected by the drop of the sea ice concentration toward 90%. The storm continued its trajectory further northeast of the N-ICE2015 region, where it gradually dissipated [*Cohen et al*., 2017] and likely caused similar sea ice deformation along its track. While there have been reports on storms and swell breaking up the summer sea ice in the central Arctic [*Asplin et al*., 2012; *Simmonds and Rudeva*, 2012], powerful winter storms north of Svalbard are climatologically exceptional [*Cohen et al*., 2017], but might occur at very high Arctic Oscillation index [*Simmonds and Keay*, 2009; *Cohen et al*., 2017]. Storms are more common in the Nordic Seas in winter, as such these events can produce significant wave energy that can propagate northward into the Arctic Ocean proper.

After the early-February storm the wind speed dropped, but the heavily deformed sea ice continued its southward drift with a very fast speed of 0.86 m/s. The distance to the ice edge dropped below 50 km and the array was hit by another storm with two distinctive peaks of strong winds lasting from 15 to 16 and again from 17 to 21 February. The first peak compressed the ice pack (negative divergence values) with southerly winds, but at the beginning of the second peak winds turned southward and the divergence gradually became positive. The ice pack stretched and finally broke up with a minor peak in shear on 18 February and a gradual increase in divergence. At this point, the array was so close to the ice edge that the breakup was possibly also assisted by swell propagating into the pack. After the breakup sea ice in the array started to oscillate between divergent and convergent motion, sea ice concentration dropped below 80% and the IMBs in the array detected bottom melt and flooding of the ice floes [*Provost et al*., 2017]. The array started to drift with high speeds (with mean at 0.93 m/s) associated with the free drift and majority of the buoys without flotation support were lost shortly afterward (Table 1).

The N-ICE2015 array deployed in spring drifted predominantly southwest with a mean speed of 0.45 m/s. The deformation time series show only two major events, both connected to storms, none of which was as powerful as any of the major winter storms. The atmospheric circulation resembled an average situation with a smaller extension of the Polar vortex [*Cohen et al*., 2017]. The atmospheric temperatures were still close to −20°C until a storm between 25 and 27 April after which the temperatures gradually increased and finally approached positive values at the beginning of June. In contrast to the winter deployment, the spring deployment shows oscillations in the divergence following the April storm (Figure 4). The oscillations have a subdaily periodicity and are not visible in the moving averages with a window of 24 h. The oscillations could be a consequence of a more open sea ice with lower internal strength, or the influence of tides as the ice drifted over Yermak plateau where tidal amplitudes are higher than over deeper surrounding ocean [*Meyer et al*., 2017]. Along with the rise of the atmospheric temperatures, mean sea ice temperatures measured by the IMBs in the array also increased from −20°C for the winter array [*Provost et al*., 2017] to −10°C for the spring array [*Itkin et al*., 2015].

Ice within the spring array broke up during the storm starting on 2 June. The breakup is associated with a series of moderate peaks in shear and divergence. During and after the storm deformation values calculated for the large triangles between the buoys began to oscillate strongly. The divergence became predominantly positive, pointing to general disintegration of the sea ice cover and coinciding with the reduction in ice concentration below 80%. Drift velocity after the breakup increased to 0.68 m/s. After 4 June, sea ice drifted into the warm ocean surface waters and began to melt rapidly from bellow, becoming nearly isothermal [*Itkin et al*., 2015].

4. Spatial Scaling Relationships and Comparison to the Other Data Sets

Sea ice deformation measured on different spatial and temporal scales, locations, and during different seasons cannot be compared directly. The power law for sea ice deformation (equation (7)) obtained through statistical analysis shows that the total deformation values (D) align along an exponential curve that decreases with increasing spatial scale (L). This makes it possible to compare the power law exponents (β) between different locations and seasons. β is essentially a measure of how well the deformations at low L transmits to the larger L − termed deformation localization. Scatter plots featuring the scaling relationship in deformation for the N-ICE2015 arrays (Figures 5a–5c) show a wide range of β. In the early part of winter deployment (prior to the February storms), β is lowest at 0.37. The exponent increases strongly (to 0.54) during and after the storms and remains similarly high during the spring deployment. Similar development is also visible directly in the deformation time series (Figure 4), where for the spring array small triangles consistently give larger average values than large triangles during peaks, while in the winter this only becomes clearly visible after the first February storm. The scatter plots also show a similar development in the level of total deformation from winter to spring at short and long scales. For example, at the length scale of 10 km the mean total deformation for the winter pre-storm conditions was 0.3 d^{-1} and 0.5 d^{-1} for the winter post-storm and 0.4 d^{-1} for the spring conditions.

The N-ICE2015 β is comparable to the values obtained from other buoy deployments (Figures 5d–5f). *Hutchings et al*. [2011] previously calculated the exponent for the SEDNA array. To eliminate the methodological differences, we recalculated the deformation rates for SEDNA using our procedures and additionally analyzed the ACSYS and DAMOCLES data. For all three buoys arrays, we assumed the same conservative positioning error as for the N-ICE2015 arrays ($\delta_x = 50m$). DAMOCLES and ACSYS buoy arrays are both missing small scale values, which could influence the steepness of the power law slope. All three earlier buoy arrays continue into the summer, but, for this paper, we analyzed data only with the time spans similar to N-ICE2015 arrays.

The earlier Arctic buoy array deployments (DAMOCLES, SEDNA, and ACSYS) all show substantially lower rates of total deformation than N-ICE2015 arrays. While the mean total deformation at 100 km length scale exceeds 0.1 d^{-1} in all three cases for N-ICE2015 scatter plots (winter pre-storm and post-storm and spring), this is not the case for any of the earlier deployments. The elevated deformation rates were also confirmed at small length scales (50 m–5 km) by the measurements based on the ship radar images [*Oikkonen et al*., 2017]. β is variable between the experiments (0.35 for DAMOCLES, 0.41 for ACSYS and 0.4 for SEDNA) and it increases southward and toward the sea ice edge, but it remains lower than the winter post-storm and spring N-ICE2015 β values of 0.54 in all the cases. This suggests that the early winter (N-ICE2015 winter pre-storm) and high north (DAMOCLES) deformation values align along a power law with a β around 0.35, while late winter and spring data sets exhibit higher values between 0.4 and 0.54. The highest values were measured while the arrays were drifting though sea ice adjacent to the marginal ice zone.

5. Discussion

Divergence and shear peak during the storms. The direction of ice drift—towards the ice edge or away from it—during the storm determines weather the deformation will on average be divergent and produce leads with open water or not. The scatter plots of the sea ice drift direction and moving averages of divergence in Figure 6 show that storms (defined here as wind speed higher than 8 m/s, circles outlined in purple) that cause easterly or southerly drift—in the case of N-ICE2015 this co-incided with directions towards the ice edge—resulted in a more divergent motion. Other storms resulted predominantly in a convergent motion.

Figure 7 shows a scatter plot of divergence versus sea ice concentration (from AMSR2; www.seaice.uni-bremen.de [*Spreen et al*., 2008]). The data from the winter array show a clear relationship between low sea ice concentration—evidence for the presence of leads—and positive divergence. A linear fit of divergence and ice concentrations higher than 80% shows that the divergent motion is shortly followed by decrease in sea ice concentration.

During the spring deployment, only one storm (the late April storm, Figure 6) caused clearly divergent conditions. Strong wind events were more evenly distributed across ice drift directions with a frequency peak

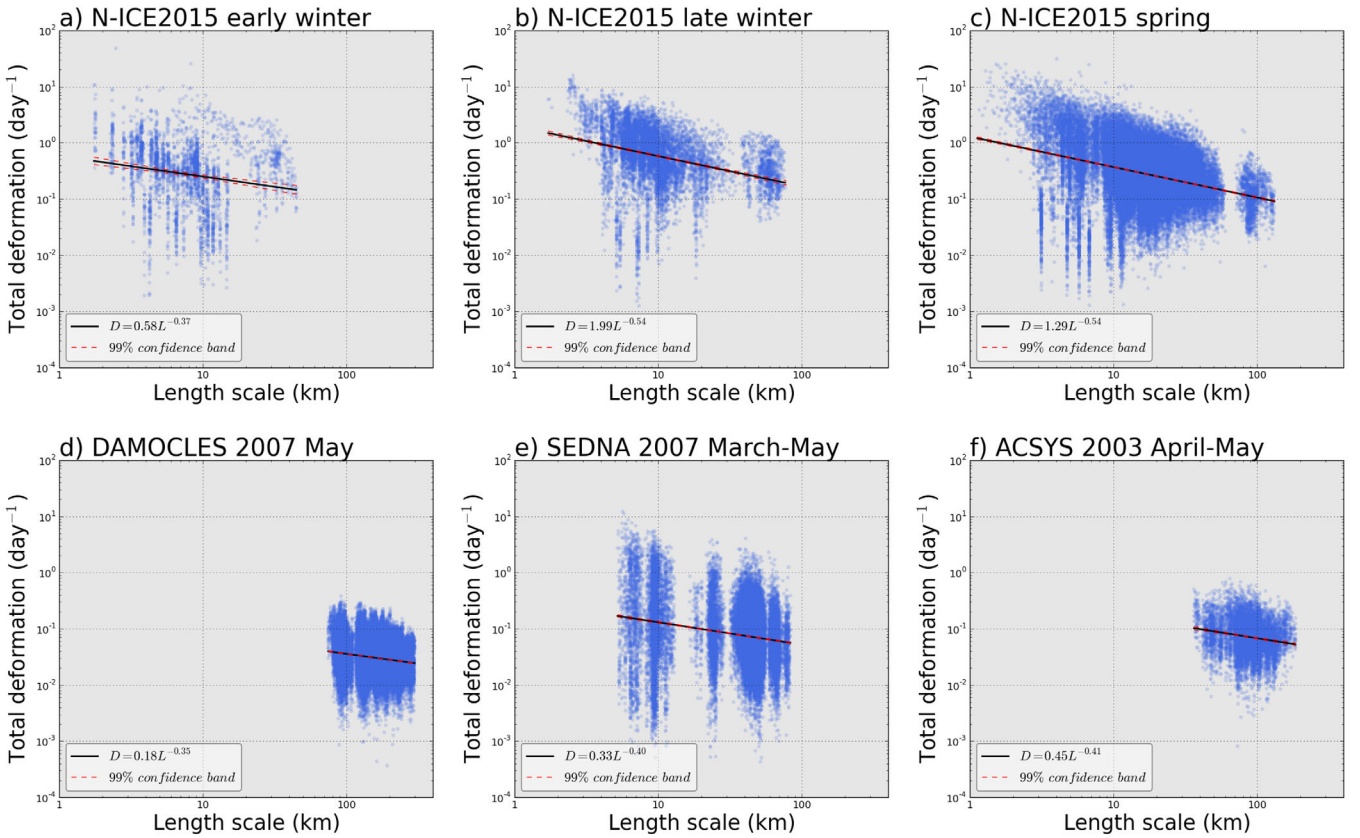

Figure 5. Scatter plots of length scale and total deformation for N-ICE2015 (a—winter before the storm, b—after the storm, and c—spring), d—DAMOCLES 2007, e—SEDNA 2007, and f—ACSYS 2003. The exponential fit to the data is depicted with the black line that follows the power law. Note the logarithmic scale on both axis. Refer to Figure 1 for locations of the array deployments.

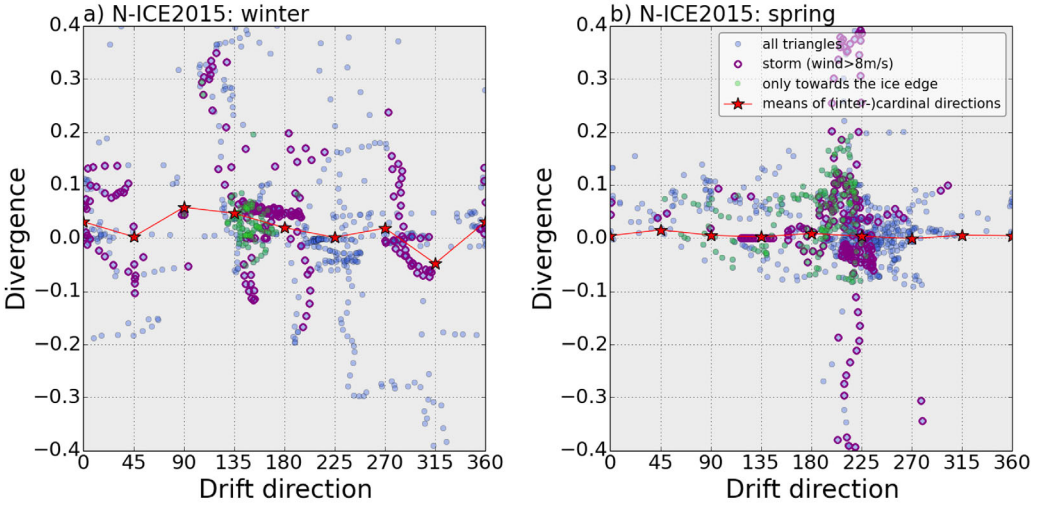

Figure 6. Scatter plots of sea ice divergence and sea ice drift angle; 0/360 is toward the north. All data points are plotted as blue circles. Storms-occasions where wind speed exceeds 8 m/s are outlined in purple. Data points where the sea ice moves toward the ice edge are overlayed by green circles. Here toward ice edge direction is sea ice drifting inside a 25° envelope around the shortest distance line from the array center to the open water. The average divergence of the intercardinal directions (N, NE, E, SE, S, SW, W, and NW) are calculated for the storm events and depicted as red stars.

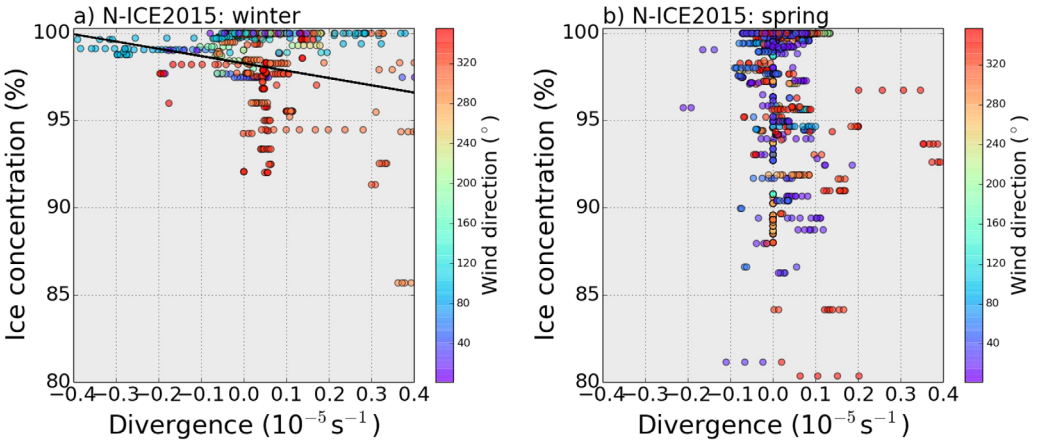

Figure 7. Scatter plots of sea ice divergence (moving averages over 24 h) versus ice concentration of the sea ice drift with the second-order polynomial fit for the sea ice concentrations lower than 100% and higher than 80%. Color of the markers is the wind direction.

at already predominant southwest drift which in average resulted in convergent motion. If these data are representative of previous years, this suggests that in the N-ICE2015 region only powerful winter storms can cause a strong divergence and shear that opens up leads. In spring conditions, when there was no such powerful storm and when the sea ice cover has been previously broken up by the winter storms, this relationship breaks down.

Although the spring array deformation time series has only a few visible events and the sea ice drift speed was lower than for the winter array, the general level of the deformation and the power law exponent remain high despite low temperatures. The reason for this might be that the spring array was deployed on sea ice that was broken up during the winter storms upstream in the Transpolar Drift and was still drifting in the N-ICE2015 region. In addition to the early February storm, there was a similarly powerful storm also in mid-March during the second drift of *Lance* [*Cohen et al.*, 2017]. During that storm no buoy array was deployed and no deformation data are available. The spring array was deployed less than 100 km upstream of the ice floe on which a meteorological mast was installed during that previous drift. There is clear increase in the wind factor (the ratio drift speed to the wind speed) during calm conditions (wind $<$8 m/s) before and after the early-February storm (Figure 8). Thus, the ice drifted faster in relation to the wind after the storm than before. This shows how the sea ice cover never recovered after the early February storm or that it was again and further damaged during the mid-March storm.

The sea ice during N-ICE2015 had a modal thickness at 0.9 m for the first year and 1.5 m for the second year ice in the winter period, and 1.7 m in spring for both ice types [*Rösel et al.*, 2016a,2016b]. This is noticeably thinner than the sea ice in which buoy arrays of SEDNA, DAMOCLES, and ACSYS were deployed

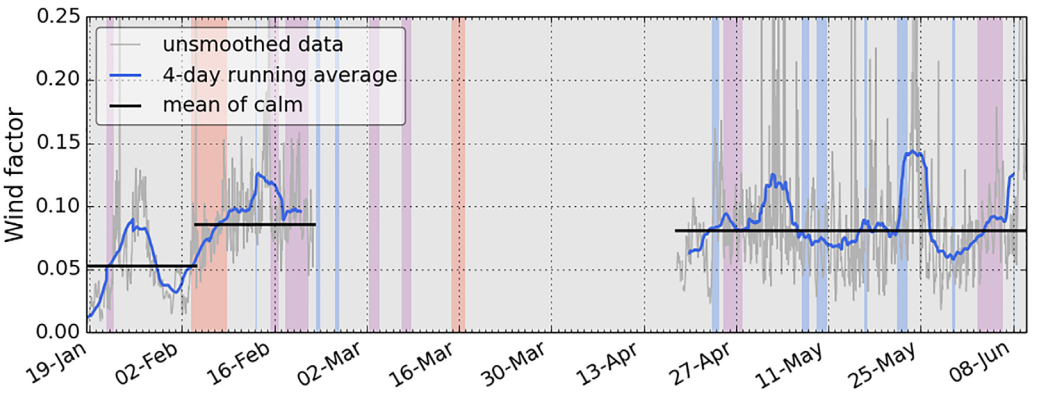

Figure 8. Time series of wind factor (drift speed/wind speed). Major and minor storms are highlighted by purple and blue shading. Most powerful storms (wind speed peak above 19 m/s and high maximum rate in air pressure decrease) are highlighted in orange.

(approximately 2 m). Furthermore, the sharp rise of the N-ICE2015 late winter array β (0.54) that remained high throughout the N-ICE2015 spring deployment indicates the importance of the high latitude penetrating winter storms for the sea ice deformation scaling. This demonstrates that the scaling law exponent β varies in space and time, and can only be used to compare ice deformation observations, which were obtained under similar conditions but at different scales.

In the N-ICE2015 region, β is exceptionally high, indicating close to free ice drift for large parts of late winter and spring 2015. During this period the wind was predominantly northerly, the sea ice was drifting toward the marginal ice zone and was not confined against any boundary. *Oikkonen et al.* [2017] analyzed a simultaneous high resolution deformation data set based on the ship radar images taken from *Lance* for a small area (15 $\times$ 15 km) in the center of the buoy array and found a gradual increase of β with decreasing distance to the ice edge. The strong increase in β and sea ice deformation overall between early and later winter can be associated with a strong storm event in the early February. All analyzed variables such as β, divergence, shear, and wind factor show a clear and irreversible change in their behavior after the initial ice breakup by this storm and the sea ice pack could not be consolidated again despite low air temperatures below -10° for the majority of the array drift until mid-May. This shows that the timing of the first winter storm that penetrates deep into the ice cover can determine the sea ice dynamic behavior on a medium to large scale adjacent to the marginal ice zone for the rest of the winter and spring. Further data collection would be necessary to explore how such a storm would affect regions in the Central Arctic where pack ice is similarly thin and young as it was in the N-ICE region but more restricted by surrounding ice and land masses.

A faster drifting more dynamic ice cover, with, e.g., more leads opening up and higher wave amplitudes, is more susceptible to lateral melt when temperatures increase [*Asplin et al.*, 2012; *Perovich et al.*, 2001]. An early observation of a powerful storm such as the one in early-February 2015 and the successive change in sea ice dynamics therefore yields potential predictability for the summer sea ice cover.

6. Conclusions

N-ICE2015 was a unique winter and spring 5 month long drift experiment in the sea ice North of Svalbard. The accompanying buoy arrays deployed to monitor the sea ice conditions and dynamics in a larger region were primarily influenced by the relatively thin sea ice cover [*Rösel et al.*, 2016a,2016b] and several exceptionally powerful winter storms [*Cohen et al.*, 2017]. This combination caused high winter sea ice deformation values that remained high even during spring, when the winds were less powerful. The sea ice in the region was likely still impacted by the previous winter storms that broke up the ice upstream of the Transpolar Drift. Previous studies have shown that the power law for the scaling of sea ice deformation becomes steeper in summer [*Stern and Lindsay*, 2009]. Our results indicate that in the "new" Arctic with now predominantly young and thin ice a powerful Arctic winter storm can have long lasting consequences for the sea ice dynamics, at least for regions such as the Northern Barents Sea or north of Svalbard, which are not confined by coastlines and allow free ice drift after a storm. Such a storm can cause steepening of the power law of deformation already in the winter and keep it high despite low atmospheric temperatures. Although storms experienced during N-ICE2015 are still unusual, another powerful storm affected the region already in December 2015 [*Boisvert et al.*, 2016] and a positive trend in moist intrusions [*Woods and Caballero*, 2016] suggests increased storm activity in this part of the Arctic in the future.

The elevated values of deformation during N-ICE2015 along with the increasing sea ice drift speed trend also show that the level of sea ice deformation in the Arctic likely have increased and will increase in the future if the ice thinning continues. This would not only contribute to reduced floe sizes, more lateral flooding, and hence stronger snow-ice formation [*Provost et al.*, 2017], but also to higher propagation of the ocean wave energy into the ice pack that causes further breakups and facilities more lateral ice melt during summer, more open water and potentially more algal blooms and associated ecosystem shifts [*Assmy et al.*, 2017; *Olsen et al.*, 2017] and would finally also influence the economic activities in the sea ice covered regions.

The N-ICE2015 winter buoy array deployment is the first extensive multidisciplinary buoy array deployed so early in the season in the Arctic and provides an extensive data set that can be used not only for analysis of the sea ice dynamics and ice mass balance [*Provost et al.*, 2017], but also for the atmosphere and ocean surface properties.

Acknowledgments

We deeply thank the crew and scientists on board *R/V Lance*. There was a huge number of people to whom we are grateful for their help with the buoy deployments, among them Bengt Rotmo, Ottar Skog, and Steinar Aksnes stand out with their efforts during the winter deployment. We also thank the crew of the ice breaker *KV Svalbard* for assisting the travel of *R/V Lance* through the pack ice and deploying and recovering some of the buoys. The buoys itself were contributed by the Norwegian Polar Institute (through Centre for Ice, Climate and Ecosystems (ICE), Research Council of Norway project STASIS (221961/F20), and ICE-ARC programme from the European Union 7th Framework Programme, grant 603887), University of Hamburg (through project DFG EXC177), Finnish Meteorological Institute, British Antarctic Survey, the Helmholtz infrastructure program FRAM of the Alfred-Wegener-Institut, and Norwegian University of Science and Technology (NTNU). This work has been supported by the Norwegian Polar Institutes Centre for Ice, Climate and Ecosystems (ICE) through the N-ICE project. P.I. was also supported by ID Arctic (funded the by Norwegian Ministries of Foreign Affairs and Climate and Environment, programme Arktis 2030). G.S. was supported by the Institutional Strategy of the University of Bremen, funded by the German Excellence Initiative. B.C. was funded by the Academy of Finland grant 283101. J.H. was funded by the Academy of Finland grant 279310. We are grateful to Jennifer Hutchings for insightful reviews and valuable advises on the buoy data processing. We thank Norwegian Meteorological Institute for ice chart data (http://polarview.met.no/) and the University of Bremen for ice concentration data (http://www.seaice.uni-bremen.de). N-ICE2015 acknowledges the in-kind contributions provided by other national and international projects and participating institutions, through personnel, equipment, and other support. All the data used in this paper are published in the Norwegian Polar Institute database http://data.npolar.no and partly also at http://www.meereisportal.de (grant REKLIM-2013-04).

References

Arctic Monitoring and Assessment Programme (AMAP) (2013), *Arctic Climate Issues 2011: Changes in Arctic Snow, Water, Ice and Permafrost. SWIPA 2011 Overview Report*, 97 pp., Arctic Monitoring and Assess. Programme (AMAP), Oslo, Norway.

Arntsen, A. E., A. J. Song, D. K. Perovich, and J. A. Richter-Menge (2015), Observations of the summer breakup of an Arctic sea ice cover, *Geophys. Res. Lett.*, *42*, 8057–8063, doi:10.1002/2015GL065224.

Assmy, P., et al. (2017), Leads in Arctic pack ice enable early phytoplankton blooms below snow-covered sea ice, *Sci. Rep.*, *7*, 40850, doi:10.1038/srep40850.

Asplin, M. G., R. Galley, D. G. Barber, and S. Prinsenberg (2012), Fracture of summer perennial sea ice by ocean swell as a result of Arctic storms, *J. Geophys. Res.*, *117*, C06025, doi:10.1029/2011JC007221.

Boisvert, L. N., A. A. Petty, and J. C. Stroeve (2016), The impact of the extreme winter 2015/16 Arctic cyclone on the Barents-Kara seas, *Mon. Weather Rev.*, *144*(11), 4279–4287, doi:10.1175/MWR-D-16-0234.1.

Cohen, L., S. R. Hudson, V. P. Walden, R. M. Graham, and M. A. Granskog (2017), Meteorological conditions in a thinner Arctic sea ice regime from winter through summer during the Norwegian Young Sea Ice expedition (N-ICE2015), *J. Geophys. Res. Atmos.*, *122*, doi:10.1002/2016JD026034.

Girard-Ardhuin, F., and R. Ezraty (2012), Enhanced Arctic sea ice drift estimation merging radiometer and scatterometer data, *IEEE Trans. Geosci. Remote Sens.*, *50*(7), 2639–2648.

Granskog, M. A., A. Rösel, P. A. Dodd, D. Divine, S. Gerland, T. Martma, and M. J. Leng (2017), Snow contribution to first-year and second-year Arctic sea ice mass balance north of Svalbard, *J. Geophys. Res. Oceans*, *122*, 2539–2549, doi:10.1002/2016JC012398.

Granskog, M. A., P. Assmy, S. Gerland, G. Spreen, H. Steen, and L. H. Smedsrud (2016), Arctic research on thin ice: Consequences of Arctic sea ice loss, *Eos Trans. AGU*, *97*, doi:10.1029/2016EO044097.

Hutchings, J. K., A. Roberts, C. A. Geiger, and J. Richter-Menge (2011), Spatial and temporal characterization of sea-ice deformation, *Ann. Glaciol.*, *52*(57), 360–368.

Hutchings, J. K., P. Heil, A. Steer, and W. D. Hibler (2012), Subsynoptic scale spatial variability of sea ice deformation in the western Weddell sea during early summer, *J. Geophys. Res.*, *117*, C01002, doi:10.1029/2011JC006961.

Itkin, P., et al. (2015), N-ICE2015 buoy data [Data set], Norwegian Polar Inst., Tromsø, Norway. [Available at https://doi.org/10.21334/npolar.2015.6ed9a8ca.]

Kauker, F., T. Kaminski, M. Karcher, R. Giering, R. Gerdes, and M. Vobeck (2009), Adjoint analysis of the 2007 all time Arctic sea-ice minimum, *Geophys. Res. Lett.*, *36*, L03707, doi:10.1029/2008GL036323.

Kimura, N., A. Nishimura, Y. Tanaka, and H. Yamaguchi (2013), Influence of winter sea-ice motion on summer ice cover in the arctic, *Polar Res.*, *32*, 8, doi:10.3402/polar.v32i0.20193.

Marsan, D., H. Stern, R. Lindsay, and J. Weiss (2004), Scale dependence and localization of the deformation of Arctic sea ice, *Phys. Rev. Lett.*, *93*, 178,501, doi:10.1103/PhysRevLett.93.178501.

Meyer, A., et al. (2017), Winter to summer oceanographic observations in the Arctic Ocean north of Svalbard, *J. Geophys. Res. Oceans*, doi:10.1002/2016JC012391, in press.

Oikkonen, A., J. Haapala, M. Lensu, and J. Karvonen (2016), Sea ice drift and deformation in the coastal boundary zone, *Geophys. Res. Lett.*, *43*, 10,303–10,310, doi:10.1002/2016GL069632.

Oikkonen, A., J. Haapala, M. Lensu, J. Karvonen, and P. Itkin (2017), Small-scale sea ice deformation during N-ICE2015: From compact pack ice to marginal ice zone, *J. Geophys. Res. Oceans*, *122*, doi:10.1002/2016JC012387.

Olsen, L., et al. (2017), The seeding of ice-algal blooms in Arctic pack ice: the multi-year ice seed repository hypothesis, *J. Geophys. Res. Biogeosci.*, *122*, doi:10.1002/2016JG003668.

Perovich, D. K., J. A. Richter-Menge, and W. B. Tucker (2001), Seasonal changes in Arctic sea-ice morphology, *Ann. Glaciol.*, *33*(1), 171–176.

Provost, C., N. Sennéchael, J. Miguet, P. Itkin, A. Rösel, Z. Koenig, N. Villacieros-Robineau, and M. A. Granskog (2017), Observations of flooding and snow-ice formation in a thinner Arctic sea ice regime during the N-ICE2015 campaign: Influence of basal ice melt and storms, *J. Geophys. Res. Oceans*, *122*, doi:10.1002/2016JC012011.

Rampal, P., J. Weiss, and D. Marsan (2009), Positive trend in the mean speed and deformation rate of Arctic sea ice, 1979–2007, *J. Geophys. Res.*, *114*, C05013, doi:10.1029/2008JC005066.

Renner, A. H. H., S. Gerland, C. Haas, G. Spreen, J. F. Beckers, E. Hansen, M. Nicolaus, and H. Goodwin (2014), Evidence of Arctic sea ice thinning from direct observations, *Geophys. Res. Lett.*, *41*, 5029–5036, doi:10.1002/2014GL060369.

Rösel, A., et al. (2016a), N-ICE2015 total (snow and ice) thickness data from EM31, doi:10.21334/npolar.2016.70352512.

Rösel, A., et al. (2016b), N-ICE2015 snow depth data with Magnaprobe, doi:10.21334/npolar.2016.3d72756d.

Simmonds, I., and K. Keay (2009), Extraordinary September arctic sea ice reductions and their relationships with storm behavior over 1979–2008, *Geophys. Res. Lett.*, *36*, L19715, doi:10.1029/2009GL039810.

Simmonds, I., and I. Rudeva (2012), The great Arctic cyclone of August 2012, *Geophys. Res. Lett.*, *39*, L23709, doi:10.1029/2012GL054259.

Spreen, G., L. Kaleschke, and G. Heygster (2008), Sea ice remote sensing using AMSR-E 89-GHz channels, *J. Geophys. Res.*, *113*, C02S03, doi:10.1029/2005JC003384.

Spreen, G., R. Kwok, and D. Menemenlis (2011), Trends in Arctic sea ice drift and role of wind forcing: 1992–2009, *Geophys. Res. Lett.*, *38*, L19501, doi:10.1029/2011GL048970.

Stern, H. L., and R. W. Lindsay (2009), Spatial scaling of Arctic sea ice deformation, *J. Geophys. Res.*, *114*, C10017, doi:10.1029/2009JC005380.

Woods, C., and R. Caballero (2016), The role of moist intrusions in winter Arctic warming and sea ice decline, *J. Clim.*, *29*(12), 4473–4485, doi:10.1175/JCLI-D-15-0773.1.

Zhang, J., R. Lindsay, A. Schweiger, and M. Steele (2013), The impact of an intense summer cyclone on 2012 Arctic sea ice retreat, *Geophys. Res. Lett.*, *40*, 720–726, doi:10.1002/grl.50190.